Acoustic Resonance of Simulated Solid Rocket Motor Chamber with Transient Sidewall Mass Additions

A. M., Hegab[#1], S. A. Gutub[*2]

[#1] *Mechanical Engineering Department, Faculty of Engineering at Rabigh,King Abdulaziz University, Saudi Arabia*

[*2]*Civil Engineering Department, Faculty of Engineering at, King Abdulaziz University, Saudi Arabia*

Abstract *An asymptotic technique is integrated with computational solution development to study the flow-field in acoustically simulated SRM chamber geometry. The computational solution is carried out for a high Reynolds number and low Mach number internal flows driven by transient side-wall mass addition in a long chamber. This kind of flow (transient, weakly viscous, and contains vorticity) have several features in common with a turbulent flow-field. Many investigations to chamber flow turbulence modelling, based on κ-ε, κ-ω and full Reynolds stress methods, have been studied. They revealed that the turbulence models, like κ-ε and κ-ω, that used to predict the turbulence level, are not very successful in predicting the transverse location of the turbulence intensity peak as well as show over predicting turbulence level than the measured values. The current study employ a full Navier-Stokes equations to analyze the RMS values for a flow in porous channel. At a higher Reynolds numbers, transition to a turbulent velocity profile is predicted. The comparison to the experimental data in cold-flow indicates agreement with the laminar description for the mean velocity profile, while the turbulence level predicted was approximately twice than the measures values.*

Keywords *Solid Rocket Motor Chamber, Unsteady Vorticity, Transient Mass Injection, Internal Cavity*
.

I. INTRODUCTION

The present numerical simulation is performed to study the flow-field in acoustically simulated SRM chamber geometry. The computational solution is carried out for a high Reynolds number and low Mach number internal flows driven by transient side-wall mass addition in a long chamber. This kind of flow (transient, weakly viscous, and contains vorticity) have several features in common with a turbulent flow-field.

Recent studies.[1-4], demonstrate that the boundary conditions of the adapted cold model simulations found to be different than the real life situation of the combustion models. As a results, we try in the current research to employ a full Navier-Stokes equations to analyze the RMS values for a flow in porous channel.

The axially distributed transverse velocity on the sidewall is a prescribed function of time with many wave numbers, [6-12]. Many studies by Flandro [13], Majdalani, Van Moorhem [14,15], and Smith et al. [17] of time dependent boundary mass addition have been surveyed. Vuillot and Avalon [16] revealed the presence of vorticity similar model.

More intensive computational techniques have been carried out by Tseng et al. [18] and Roh and Yang [19] to include the reactive models.

Many investigations to chamber flow turbulence modeling, based on κ-ε, κ-ω and full Reynolds stress methods, have been studied. Liou and Lien, [29] revealed that the turbulence models, like κ-ε and κ-ω, that used to predict the turbulence level, are not very successful in predicting the transverse location of the turbulence intensity peak as well as show overpredicting turbulence level than the measured values. For example, Beddini, [30], employed a full Reynolds stress turbulence model to analyze the flow in porous channel. At a higher Reynolds numbers, transition to a turbulent velocity profile is predicted.

The results by Sabnis et al., [31] using the low Reynolds number κ-ε turbulence model show greatly overpredicting turbulence levels but indicates agreement with the experimental data for the axial mean velocity profiles. In general, in spite of the overpredicting turbulence level and the unsuccessful in predicting the transverse location of the turbulence peak, the turbulence models proved satisfactory in the pretransition region of the mean-flow.

Related numerical calculations have been carried out by Tseng et al. [18] and Roh and Yang [19] to include the effect of exothermic combustion reactions adjacent to the sidewall. The temperature variations observed in these studies arise from flame zone effects, rather than the acoustic disturbance-injected fluid interaction mentioned previously. Time-dependent numerical data by Hegab [20] and Hegab and Kassoy [6] is used to calculate the mean axial velocity distribution across the channel.

"The computational results in the present work elucidate the transient variation of the spatially distributed vorticity and temperature distribution in a channel after time-dependent mass addition from the sidewall is initiated. These results verify that relatively large vorticity and temperature gradients are present throughout the flow field although the temperature disturbances themselves are small at both resonance and non-resonance frequencies. Reflection-preserving numerical boundary conditions are used to

ensure that the computed acoustic field is an accurate solution to the posed initial-boundary value problem. In particular, the present acoustic response includes eigenfunctions predicted by Staab et al. [9] as well as the forced modes seen in Kirkkopru et al. [7] . All earlier computational studies cited here are missing eigenfunction responses that are predicted by analogous acoustic analysis for the semi-confined systems considered.

Results are given for a nondimensional sidewall injection distribution composed of a steady spatially uniform part and a similar amplitude oscillatory part that is axially distributed with different wave numbers. The amplitude of the latter is large enough to ensure that fully nonlinear fluid dynamics is evolving in the flow field (Staab et al [9]). Comparisons of time-evolution of temperature gradient, and vorticity distributions for non-resonant, near resonant, and at resonance oscillation frequencies are used to show how relatively large amplitude disturbances evolve in the latter case. The results of the present study show that surprisingly large transient vorticity and temperature gradients are present on the sidewalls and in the interior of the channel, at the resonance frequency and low wave number even when the transverse fluid injection is isothermal. This unexpected phenomenon arises from an interesting interaction between acoustic disturbances present in the low Mach number internal flow and the isothermal fluid injected from the boundary.

The observed axial variation in the radial temperature distribution is explained in terms of the acoustic-injected fluid interaction derived in the asymptotic analyses of Staab et al. [9], Rempe et al. [10] and Zhao et al. [11,12]. Related ideas are used to show why the axial distribution of the temperature, temperature gradient, and vorticity is sensitive to the wave numbers of the axial variation of the injection velocity.

This document is a template. An electronic copy can be downloaded from the conference website. For questions on paper guidelines, please contact the conference publications committee as indicated on the conference website. Information about final paper submission is available from the conference website"[27,32].

II. The Physical and Mathematical Formulation

The mathematical model is written as;

$$\frac{\partial Q}{\partial t}+\frac{\partial E}{\partial x}+\frac{\partial F}{\partial y}=0 \quad , \tag{1}$$

where;

$$Q=\left[\rho,\rho u,\rho v,E_T\right]^T ,$$

$$E=\left[M\rho u, M\rho u^2+\frac{1}{\gamma M^2}p, M\rho uv, M\{E_T+(\gamma-1)p\}u\right]^T$$

$$F=\left[M\rho v, M\rho uv-\frac{\delta^2 M}{R_e}u_y, M\rho v^2+\frac{\delta^2}{\gamma M}p, M\{E_T+(\gamma-1)p\}v-\frac{\gamma\delta^2 M}{R_e P_r}T_y\right]^T$$

ET is the total energy ($\rho[T+\gamma(\gamma-1)M^2(u^2+(v/\delta)^2]$) and the equation of state for a perfect gas is;

$$p=\rho T \tag{2}$$

with the non-dimensional quantities;

$$p=p^{'}/p_o^{'},\ \rho=\rho^{'}/\rho_o^{'},\ T=T^{'}/T_o^{'},$$

$$u=u^{'}/U_{z_o}^{'},\ v=v^{'}/\left(U_{z_o}^{'}/\delta\right),$$

$$x=x^{'}/L^{'},\ y=y^{'}/H^{'},\ t=t^{'}/t_a^{'} \tag{3}$$

$$M=\frac{U_{z_o}^{'}}{C_0^{'}},\quad P_r=\frac{\mu_0^{'}C_{p_o}^{'}}{k_0^{'}},\quad R_e=\frac{\rho_0^{'}U_{z_o}^{'}L^{'}}{\mu_0^{'}},\ \text{and}\quad R_{e_A}=\frac{R_e}{M} \tag{4}$$

Parameters ranges of interest include M≤ O(10-1) and Re=O(10^5-10^6)

A. The Initial and Boundary Conditions

The axial variation, time-dependent injection transverse is imposed with the boundary and initial conditions for the steady and unsteady flows can be written as follows;

x=0; u = 0, v = 0. (5)

x=1; p = 1, "pressure node" (6)

y=0;

$$v=0,\ \frac{\partial u}{\partial y}=\frac{\partial T}{\partial y}=\frac{\partial p}{\partial y}=\frac{\partial \rho}{\partial y}=0 \tag{7}$$

y=1; u=0, T=1,

and

$$v=\begin{cases}-v_{rws}(x) & t\le 0,\\ -v_{rws}(x)-\varepsilon\varphi_{rw}(1-\cos\omega t) & t>0,\end{cases} \tag{8}$$

t=0; u=v=0, p=T=1

(9)

The Analytical Approach

Staab et al. [9] show that;

$$(u,v,P,\rho,T)=(u_s,v_s,P_s,\rho_s,T_s)+\left(\hat{u},\hat{v},\hat{P},\hat{\rho},\hat{T}\right) \quad (10)$$

The asymptotic expansions for the velocity components and the thermodynamic variables in the limit M→0 are;

$$u(x,y,t)\sim u_{os}(x,y)+\sum_{n=0}^{\infty}M^n\hat{u}_n(x,y,t),\ v(x,y,t)\sim v_{os}(x,y)+\sum_{n=0}^{\infty}M^n\hat{v}_n(x,y,t), \quad (11)$$

$$P(x,y,t)\sim P_{os}(x,y)+\sum_{n=0}^{\infty}M^{n+1}\hat{P}_n(x,y,t),\ T(x,y,t)\sim T_{os}(x,y)+\sum_{n=0}^{\infty}M^{n+1}\hat{T}_n(x,y,t),$$
$$\rho(x,y,t)=P(x,y,t)/T(x,y,t),\ \hat{P}_o=\hat{\rho}_o+\hat{T}_o \quad (12)$$

The final derived form can be written as follows;

$$\frac{1}{\gamma}\int_{y=0}^{1}\left(\frac{\partial^2\hat{P}_0}{\partial t^2}-\frac{\partial^2\hat{P}_0}{\partial x^2}\right)dy=-\int_{y=0}^{1}\frac{\partial}{\partial y}\left(\frac{\partial\hat{v}_o}{\partial t}\right)dy \quad (13)$$

The thermodynamic variables in the limit M→0 are;

$$u(x,y,t)\sim u_{os}(x,y)+\sum_{n=0}^{\infty}M^n\hat{u}_n(x,y,t),\ v(x,y,t)\sim v_{os}(x,y)+\sum_{n=0}^{\infty}M^n\hat{v}_n(x,y,t), \quad (14)$$

$$P(x,y,t)\sim P_{os}(x,y)+\sum_{n=0}^{\infty}M^{n+1}\hat{P}_n(x,y,t),\ T(x,y,t)\sim T_{os}(x,y)+\sum_{n=0}^{\infty}M^{n+1}\hat{T}_n(x,y,t),$$
$$\rho(x,y,t)=P(x,y,t)/T(x,y,t),\ \hat{P}_o=\hat{\rho}_o+\hat{T}_o \quad (15)$$

The resultant equation can be written as follows;

$$\frac{1}{\gamma}\int_{y=0}^{1}\left(\frac{\partial^2\hat{P}_0}{\partial t^2}-\frac{\partial^2\hat{P}_0}{\partial x^2}\right)dy=-\int_{y=0}^{1}\frac{\partial}{\partial y}\left(\frac{\partial\hat{v}_o}{\partial t}\right)dy \quad (16)$$

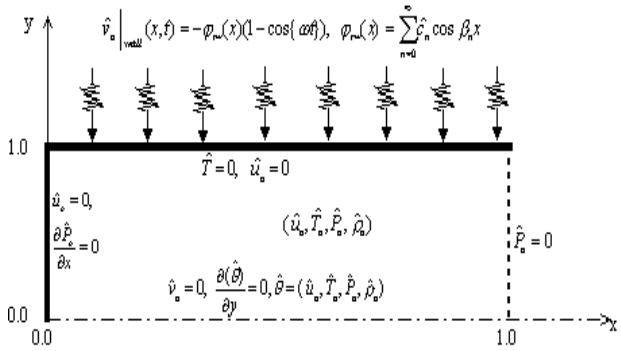

Figure 1: The boundary conditions for the perturbed flow variables that superimposed on the converged steady state solutions.

$$t=0,\quad \hat{P}_o=0,\quad \frac{\partial\hat{P}_o}{\partial t}=0 \quad (17)$$

$$x=0,\quad \frac{\partial\hat{P}_o}{\partial x}=0,\quad x=1,\quad \hat{P}_o=0 \quad (18)$$

y=0;

$$\hat{v}_0=0, \quad (19)$$

y=1

$$\hat{v}_o=-\varepsilon\varphi_{rw}(1-\cos\omega t)\qquad t>0, \quad (20)$$

Using the boundary conditions at y=0,1, the equation (16) can be written as;

$$\frac{\partial^2\hat{P}_0}{\partial t^2}-\frac{\partial^2\hat{P}_0}{\partial x^2}=\gamma\,\omega\,\varepsilon\,\varphi_{rw}(x)\sin\omega t \quad (21)$$

Equation (21) represents the wave equation for the acoustic pressure fields.

B. The Computational Approach

The present study employs higher order accuracy difference equations in MacCormack[21], Gottlieb et al.[22], and Poinson, et al. [23] is used to solve the 2-D, unsteady, compressible Navier-Stokes equations at the interior points and at the boundaries.

The mass conservation is satisfied using the condition:

$$\left(\phi_{i,j}^{t+1}-\phi_{i,j}^{t}\right)\approx 10^{-k} \quad (22)$$

where ϕ=(u,v,p,T) and k is an arbitrary coefficient based on the solution precision. Typical values of k ≤ 10^{-4}. More details about the computational approach is found in [27,32].

III. Results and Discussions

The objective of this work is to study the influence of different flow parameters and their RMS values on the nature of the flow field inside the SRM chamber.

A. *Code Validation*

The current code has been verified in figure (2) by comparing our results with the analytical and the experimental results by Deng, et.al. [24, 25] for the steady state solution. The results shows good agreement with a certain deviation between the experimental and the theoretical approach..

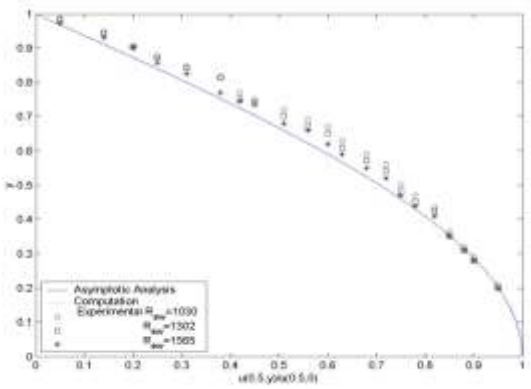

Figure (2) : Normalized axial velocity profiles at the midlength of the chamber for the steady state flow, [27,32].

The steady state velocity vector map at t=0 is presented in Fig. (3). It is noted that these vectors is qualitatively closer to the experimental flow pattern by Deng, and the coworker in particular in case of less turbulence with the pore size 1/8" honeycomb.

Figure(3) : Instantaneous velocity vector map at t=0.0

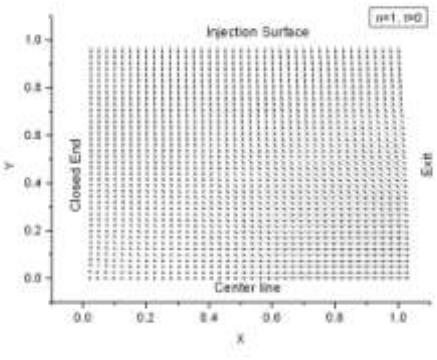

A comparison of the analytical temperature time history ($\hat{T}$), with the numerical solution in figure(4) show reasonable agreement between the analytical and computational solutions.

Moreover a comparison of the asymptotic analysis perturbed pressure time history with the computational one at and near resonance frequencies is presented in Fig. (5). For t< 10 the results show good agreement between the two approaches even with the asymptotic beat condition

$$(\omega = \pi/2 - 0.0018)$$

which is very close to the resonance frequency. While for t>10 the asymptotic solution show linear growth with time based on the linear theory for the derived wave equation, where

$$\omega = \beta_{n^*} = \pi/2$$

In contrast, the computational solution show beats at the resonance condition due to the nonlinearity and the asymptotic beat solution have a smaller amplitude than the resonance one. The beats appear due to the interaction between the deriving frequency mode

$$\omega = \pi/2 - 0.0018$$

and the first eigenfunction mode (π/2)".

Figure(4) : Comparison between the computational

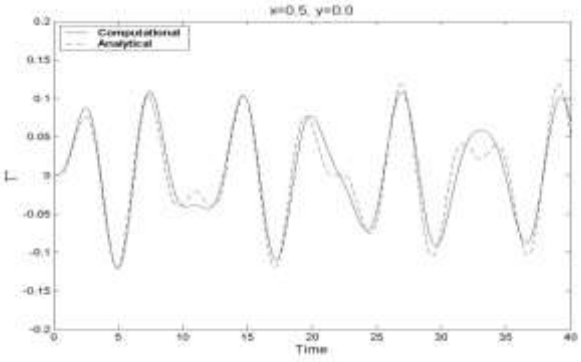

and the asymptotic solutions for the perturbed temperature time history with ω =1 (non-resonance), ε=0.4, M=0.02, and Re=3*105 at the half-length of the chamber, [27,32].

Figure(5) : Comparison between the computational and the asymptotic solutions for the perturbed pressure

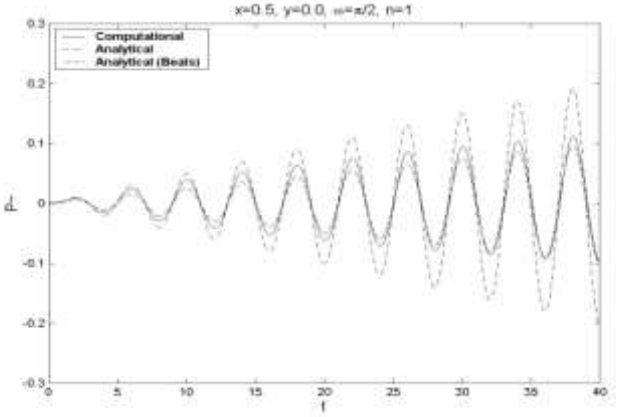

time history with ω =π/2 (resonance) , ε=0.4, M=0.02, and Re=3*105at the half-length of the chamber

Turbulence Characteristics Results

The complete axial unsteady velocity in the chamber can be divided into the mean motion and into fluctuation as,

$$u = < u > + u_p^{`} + u_v^{`} \tag{23}$$

Where

$u_p^{`}$ is the acoustic fluctuation,

$u_v^{`}$ is the rotational fluctuation, and < > denotes the time-averaging.

The RMS of the axial fluctuation intensity is defined as,

$$\left[< \left(u_p^{`} + u_v^{`}\right)\left(u_p^{`} + u_v^{`}\right) > \right]^{1/2} = \left[< u_p^{`} u_p^{`} > + 2 < u_p^{`} u_v^{`} > + < u_v^{`} u_v^{`} > \right]^{1/2} \tag{24}$$

The time-averages at a fixed point,

$$< \alpha > = 1/T \int_o^T \alpha dt \tag{25}$$

are given over a long period "T" to ensure that the vorticity fills the entire chamber. α represents the flow parameters and the mixed products.

The total RMS intensity for ω = π/2 and ε=0.4, M=0.02, and RE=3*10^5 as in equations (23-25) is presented in figure (6).

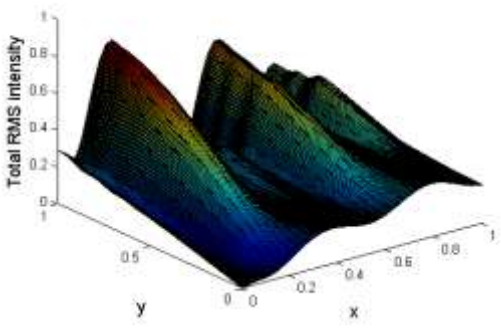

Figure(6) Total RMS intensity for ω = π/2 and ε=0.4, M=0.02, and R_E=3*10^5

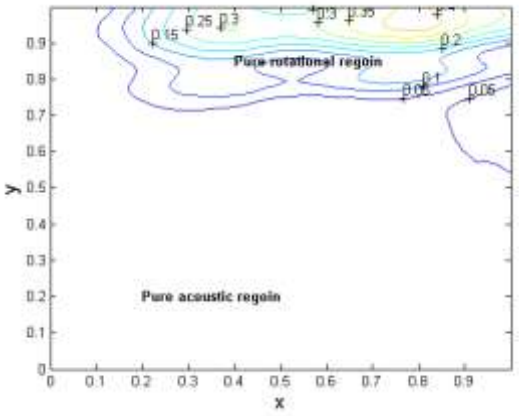

Figure(7) Pure rotational and irrotational regions with the same parameters as in Fig.(6)

The pure rotational and irrotational regions is presented in Fig.7 for the same parameters as in Fig. (6).

More results for the Reynolds stress obtained from the time-average of the mixed product of velocity fluctuation, <u`v`> for Re=4*105 , M=0.02, A=20, n=1, ε=0.4, and ω=1 is obtained. The product <u`v`> represents the transport of the x-momentum through a surface normal to the y-axis and defines an additional stress arising from the fluctuations on the mean motion. The stress has significant negative values at the midchamber adjacent to the wall. If a particle with v`<0 moves into a region where

$\frac{\partial < u >}{\partial y} < 0$, then the corresponding u`>0 and vice versa.

This means that the time-average of the mixed product of the velocity fluctuation, <u`v`>, is always negative. The transverse gradient <u`v`> fluctuates from positive to negative across the chamber. In addition the maximum amplitude of the Reynolds stress occurring adjacent to the propellant surface may also impact the burning rate of a solid propellant.

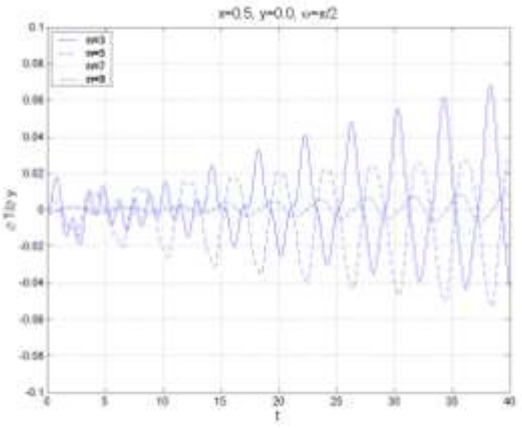

Figure (8) The heat transfer variation at resonance for four eigenvalues.

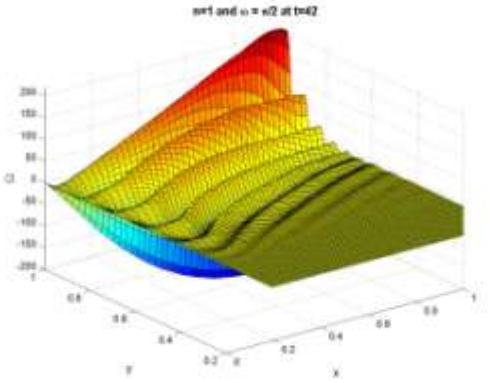

Figure (9) The shear stresses variations at resonance at t=42.

More results about the variation of the heat transfer effects and the vorticity variation at resonance is presented in figures (8) and (9).
The beat response is observed at this frequency in the case of nonlinear, weakly viscous acoustic-flow. The beat response may arise from the interaction between the forcing oscillation at the driving frequency and the first fundamental mode. In addition, the oscillations amplitude is greater than for ω=1.

IV. Conclusions

Results of the kind described here may help to identify high heat transfer and erosional burning location in motor chambers. The RMS values show that the vorticity and the associated rotational and thermal flow is generated at the side wall and fill the entire chamber as time increases. The idea here is account for the "scouring" effect of oscillatory shear stress on the fizz-foam zone thought to exist at the gas-propellant interface. Near the resonance frequency, the maximum amplitude of the intensive vorticity is greater than that for ω=1. This related to the axial acoustic pressure response, induced and sustained by the sidewall injection, which shows a large amplitude oscillations (beat) with ω=1.5, compared to the solution with ω=1. In addition a stronger peak shifts toward the side wall injection than that for ω=1. Moreover, The beat response is observed at this frequency in the case of nonlinear, weakly viscous acoustic-flow. The beat response may arise from the interaction between the forcing oscillation at the driving frequency and the first fundamental mode. In addition, the oscillations amplitude is greater than for ω=1.

V. Acknowledgment

Hegab, A.M., would like to thank Prof. D.R. Kassoy, University of Colorado at Boulder, USA for his cooperation.

VI. References

[1] Hegab A., Buckmaster J., Jackson T., and Stewart, S. "The Burning of Periodic Sandwich Propellants" AIAA Paper #2000-3459, 36th. AIAA/ASME/SAE/ASEE Joint Propulsion, July 17-19, 2000, Huntsville, Al., USA

[2] Hegab A., Jackson T., Buckmaster J., Stewart D., (2001) "Nonsteady Burning of Periodic Sandwich Propellants with Complete Coupling between the Solid and Gas Phases", Journal of Combustion and Flame, 125, 1055-1070, 2001.

[3] Buckmaster J., Jackson T., Hegab A., Kochevets S., Ulrich M. (2001) "Randomly Packed Heterogeneous Propellants and the Flame They Support" AIAA paper 2001-0337, 39th. Aerospace Science Meeting, Reno, NV, USA.

[4] Kochevets S., Buckmaster J., Jackson T., Hegab A. (2001) "Random Propellant Packs and the Flame they Support" Journal of Propulsion and Power, Vol. 17(4), pp 883-891.

[5] Hegab, A.M. (2003), " Numerical Flow Temperature Dynamics in Channel with Time-Dependent Mass Injection" Sci. Bull. Faculty of engineering, Ain Shams University, ISSN 1110-1385, pp 743-764.

[6] Hegab, A.M. and Kassoy, D.R. (2006), "Internal Flow Temperature and Vorticity Dynamics in Channel with Transient Mass Addition" AIAA Journal, Vol.44, No.4, April 2006, pp 812-826.

[7] Kirkkopru, K., Kassoy, D.R., and Zhao, Q. (1996), " Unsteady Vorticity Generation and Evaluation in a Model of Solid Rocket Motor," J. of Propulsion and Power, 12, No. 4, 646-654.

[8] Kirkkopru, K., Kassoy, D.R., Zhao, Q., and Staab, P. (2000), " Acoustically generated unsteady vorticity field in along narrow cylinder with sidewall injection," submitted to J. Eng. Math.

[9] Staab, P.L., Zhao, Q., Kassoy, D.R., Kirkkopru, (1999), "Co-existing Acosutic- Rotational Flow in a Cylinder with Axisymmetric Sidewall Mass Addition", Physics of Fluids, 11, 10, 2935-2951.

[10] Rempe M., Staab, P.L., and Kassoy, D.R. (2000), "Thermal Response for an Internal Flow in a Cylinder with Time-Dependent Sidewall mass Addition", AIAA 2000-0996, 38th Aerospace Science Meeting, Reno, NV.

[11] Zhao, Q., and Kassoy, D.R. (1994), "The generation and Evolution of Unsteady Vorticity in a Solid Rocket Engine Chamber," AIAA Paper 94-0779, 32th Aerospace Sciences Meeting, Reno, NV.

[12] Zhao, Q., Staab, P.L., Kassoy, D.R., and Kirkkopru, K. (2000), "Acoustically Generated Vorticity in an Internal Flow," J. Fluid Mech., #13, 247-285.
[13] Flandro, (1995), " Effect of Vorticity on Rocket Combustion Stability" Journal of Propulsion and Power, Vol. 11, 607-625.
[14] Majdalani and Van Moorhen (1997), "Multiple-Scale Solution to the Acoustic Boundary Layer in Solid Rocket Motors", Journal of Propulsion and Power, Vol. 13, 186-193.
[15] Majdalani and W. Van Moorhen (1998), "Improved Time-Dependent Flow Field Solution for Solid Rocket Motors", AIAA Journal, 36, 241-248.
[16] Vuillot, F., and Avalon, G. (1991), " Acoustic Boundary Layers in Solid propellant Rocket Motors Using Navier-Stokes Equations," J. Propulsion and Power, 7, No.1 231-239.
[17] Smith, T.M., Roach, R.L., and Flandro, G.A. (1993), "Numerical Study of the Unsteady Flow in a Simulated Solid Rocket Motor," AIAA Paper, 93-0112, 31th Aerospace Science Meeting, Reno, NV.
[18] Tseng, C.F., and Tseng. I.S.,(1994), "Interaction Between Acoustic Waves and Premixed Flames in Porous Chamber," AIAA 94-3328, 32th Aerospace Science Meeting, Reno, NV.
[19] Roh, T.S., and Yang, V. (1995), "Transient Combustion Responses of Solid Propellants to Acoustic Disturbances in Rocket Motors," AIAA Paper, 95-0602, 33th Aerospace Science Meeting, Reno, NV.
[20] Hegab, A.M. (1998) "A Study of Acoustic Phenomena in Solid Rocket Engines", Ph.D. Thesis, Mech. Power Engineering Dept., Menoufia Univ., Egypt, (Carried out at the University of Colorado at Boulder).
[21] MacCormack, R.W. (1982), " A Numerical Method for Solving the Equations of Compressible Viscous Flow," AIAA J., 20, No. 9, 1275-1281.
[22] Gottlieb, D., and Turkel, E. (1976) "Dissipative Two-Four Methods for Time-Dependent problems," Mathematics of Computation, 30, No. 136, 703-723.
[23] Poinsot, T.J., and Lele, S.K. (1992), "Boundary Conditions for Direct Simulations of Compressible Viscous Flows," J. of Computational Physics, 101, 104-129.
[24] Deng, Z., Adrian, R.J., Tomkinsm C.D. (2001), "Structure of Turbulence in Channel Flow with a Fully Transpired Wall", AIAA Paper 2001-1019, 39th Aerospace Science Meeting ,Reno, NV.
[25] Deng, Z., Adrian, R.J., Tomkinsm C.D. (2002) "Sensitivity of Turbulence in Transpired Channel to Injection Velocity Small-Scale Nonuniformity", Journal of AIAA, Vol. 40, No. 11, November, 2002.
[26] Culick, F.E.C. (1966), "Rotational Axisymmetric Mean Flow and Damping of Acoustic Waves in a Solid Propellant Rocket," AIAA J. 4, No. 8, 1462-1464.
[27] A.M. Hegab, Vorticity Generation and Acoustic Resonance of Simulated Solid Rocket Motor Chamber with High Wave Number Wall Injection, J. of Computers & Fluids, Vol. 38(2009) 1258-1269.
[28] Anoop Thankachen, Santosh kumar, (2015), "Design Optimization and Analysis of Rocket Structure for Aerospace Applications", Volume-24 Number-6, International Journal of Engineering Trends and Technology (IJETT)
[29] Liou, T. M. and Lien, W. Y. (1995), " Numerical Simulations of Injection Driven Flow in a Two-Dimensional Nozzleless Solid Rocket Motor," J. of Propulsion and Power Vol. 11, No. 4, 600-606
[30] Beddini, R. A. (1986), " Injection-Induced Flows in Porous-Walled Ducts," AIAA J. Vol. 24, No. 11, 1765-1773
[31] Sabnis, J. S., Gibeling, H. J., and McDonald, H. (1989), "Navier-Stokes Analysis of Solid Propellant Rocket Motor Internal Flows," J. of Propulsion and Power Vol. 5, 637-664.
[32] Hegab, A.M., " Vorticity Generation and Acoustic Resonance of Simulated Solid Rocket Motor Chamber with Transient Sidewall Mass Injection", Proceedings of the Ninth International Congress of Fluid Dynamics & Propulsion, ICFDP9-265 December 18-21, 2008, Alexandria, Egypt